






Very Accurate Time-Frequency Representation of Induction Motors Harmonics for Fault Diagnosis Under Load Variations

Jorge Bonet-Jara , Vanessa Fernandez-Cavero , Francisco Vedreno-Santos , Daniel Morinigo-Sotelo , *Member, IEEE*, and Joan Pons-Llinares , *Member, IEEE*

Abstract—Induction motors work under steady-state in many applications. Nevertheless, in some cases they experience periodic load fluctuations, which generate constant frequency harmonics close to variable frequency bar breakage harmonics. In these cases, time-frequency (t-f) transforms are better suited than steady-state analysis since the fault harmonic frequencies change in time. Even if the healthy and faulty frequencies do not overlap in the spectrum, if the speed is unknown, it is difficult to distinguish the constant frequency healthy harmonic from the variable frequency bar breakage harmonic. On the other hand, transient techniques present in technical literature are not precise enough to deal with both the changing frequency of the bar breakage harmonic and a close constant frequency (as the one generated by most of the periodic load fluctuations). To achieve reliable results under these challenging situations, a very precise time-frequency transform must be used, enabling to simultaneously draw the constant and variable frequencies, even if they are very close in the t-f plane. The Dragon-Transform is here proposed to address the problem. It is shown through simulation and experimental results, how it enables to very accurately plot up to five faulty harmonics evolutions, distinguishing at the same time the constant frequency of the load oscillation, traced as a very thin horizontal line. Precision is so high that even the oscillations caused by ripple effect can be observed for the first time in technical literature, enhancing the reliability of the diagnosis performed, and opening the path for a true solution of the problem.

Index Terms—Induction motors, load oscillations, signal analysis, time-frequency transforms, fault diagnosis.

I. INTRODUCTION

ELECTRICAL machines are integral in both manufacturing and transport sector. Two primary types, synchronous and induction machines, dominate over the rest. Synchronous machines are favoured in industrial settings where precise control over speed and position is imperative. Conversely, induction machines find preference in scenarios where stringent speed accuracy is less critical. Given that numerous industries operate with modest speed requirements, induction machines typically emerge as the preferred choice [1].

Induction motors encounter different operational setups based on the nature of the load. When a constant load suffices without requiring precise speed control, these motors are directly connected to the grid. Contrarily, if the industrial process demands specific speeds, Variable Speed Drives, (VSDs) are employed to regulate the motor's pace. However, even in grid-fed operations, load variations may arise, impacting the motor's speed. This effect can be particularly pronounced in specific applications such as pulp mixers within the paper industry or trunk cutters in wood processing, where load fluctuations can significantly influence the motor's performance.

When induction motors function under constant loads, their speed remains stable, allowing the conventional Fast Fourier Transform (FFT) technique to diagnose them effectively by analyzing the spectrum of their stator currents. However, fault related frequencies are intrinsically tied to the motor's speed, making it imperative, as emphasised in [2], to accurately measure or estimate the motor's speed. This step is crucial for precisely pinpointing these fault-related frequencies within the frequency spectrum, quantifying their amplitudes, ascertaining the presences and severity of any faults, and facilitating accurate diagnosis.

Load variations impose considerable stress on induction machines, elevating the likelihood of failure occurrences. These fluctuations directly influence the machine's speed, resulting in varying fault frequencies that hinder precise diagnosis through FFT current spectrum analysis. Moreover, mechanical load variations mimic fault defects, heightening the probability of false-positive diagnoses [3].

Manuscript received 21 November 2023; revised 27 January 2024; accepted 26 February 2024. Date of publication 29 February 2024; date of current version 21 May 2024. Paper 2023-EMC-1291.R1, presented at the 2022 International Conference on Electrical Machines, Valencia, Spain, Sep. 05–08, and approved for publication in the IEEE TRANSACTIONS ON INDUSTRY APPLICATIONS by the Electric Machines Committee of the IEEE Industry Applications Society [DOI: 10.1109/ICEM51905.2022.9910768]. This work was supported in part by the CRUE-Universitat Politècnica de València and in part by the Spanish Ministry of Science, Innovation and Universities under Grant FPU19/02698. (*Corresponding author: Jorge Bonet-Jara.*)

Jorge Bonet-Jara and Joan Pons-Llinares are with the Instituto de Tecnología Eléctrica, Universitat Politècnica de València, 46022 València, Spain (e-mail: jorboja@die.upv.es; jpons@die.upv.es).

Vanessa Fernandez-Cavero is with the Área de ingeniería eléctrica, Departamento de ingeniería electromecánica, Universidad de Burgos, 09006 Burgos, Spain (e-mail: vfcavero@ubu.es).

Francisco Vedreno-Santos is with the School of Engineering and Built Environment, Edinburgh Napier University, EH11 4BN Edinburgh, U.K. (e-mail: F.VedrenoSantos@napier.ac.uk).

Daniel Morinigo-Sotelo is with Research Group ADIRE-HSPDigital, Institute of Advanced Production Technologies, Universidad de Valladolid, 47011 Valladolid, Spain (e-mail: daniel.morinigo@uva.es).

Color versions of one or more figures in this article are available at <https://doi.org/10.1109/TIA.2024.3371393>.

Digital Object Identifier 10.1109/TIA.2024.3371393

The technical literature for the diagnosis of electrical machines under variable loads can be classified into three big groups. The first group includes techniques based in signal demodulation [4], [5], [6], [7], [8], [9], [10], [11], [12] which are less computationally demanding as they tend to focus on a specific harmonic or frequency bandwidth of the stator current spectrum. The second group contains time-frequency analysis techniques [13], [14], [15], [16], [17], [18], [19], [20] which require a greater computational time than signal demodulation techniques but offer a global view of all the current harmonics in the current spectrum. The third group employs alternative techniques, [21] and [22], which do not fulfil in the two previous categories.

One of the first signal demodulation techniques for the diagnosis of induction machines under transient states is presented in [4] where rotor asymmetries in an induction motor fed from a Variable Speed Drive (VSD) are diagnosed. The diagnostic technique is carried out by acquiring the current and speed of the machine under an acceleration ramp of 5 Hz/s but the slip speed, which determines the actual fault frequency, is constant around 2 Hz. Then, the stator current is demodulated by a frequency shifting what allows the analysis of the current as if the machine was operating under short stationary regimes.

The frequency shifting idea presented in [4] is further developed in [5], [6], [7], where double fed induction motors are diagnosed, [8], where a squirrel cage induction machine is diagnosed, [9], where outer broken bars of a double cage squirrel cage induction motor is diagnosed and, [10], where a rotor asymmetry in a Wound Rotor Induction Machine (WRIM) is diagnosed. In [5], [6], [7], [8], [9], [10] the Wavelet Transform (WT) and the Discrete Wavelet Transform (DWT) are employed for the extraction of the fault component from the stator current and the machines are subjected to acceleration or deceleration ramps which cause a fault frequency change of 4.44 Hz/s [5], [6], [7], [8], [9] and 0.93 Hz/s in [10]. The difference between these publications is how the energy of the frequency band extracted by the WT is computed to determine the existence or not of a fault. However, all these techniques share the same drawback: they assume that the increase of the energy in the extracted frequency band is only due to the existence of a fault component. Therefore, if there is a change in the load conditions of the induction machine the energy of the extracted frequency band can increase causing false positives.

To overcome the false positive problem an improvement to the techniques presented in [5], [6], [7], [8], [9], [10] is developed in [11], where the eccentricity fault is diagnosed, and [12], where the rotor and stator asymmetries are diagnosed, by calculating the Instantaneous Frequency (IF) of the extracted frequency band. In [11] and [12] the machines diagnosed are subjected to random increasing and decreasing speed ramps which cause a fault frequency change of 0.42 Hz/s and 1.66 Hz/s respectively. The computation of the IF of the extracted frequency band combined with the measurement of the speed in [11] and [12] allows to discern whether the energy in it is due to a fault or due to other external factors, such as oscillating loads, overcoming the main drawback, false positives, of [5], [6], [7], [8], [9], [10] at the expense of requiring a speed measurement.

One of the first publications using time-frequency analysis techniques for the diagnosis of broken bars and bearing faults in induction machines is presented in [13]. The fault diagnosis is carried out by the computation of the Short Time Fourier Transform (STFT). In [14] the diagnosis of the eccentricity fault in induction machines is performed through the Wigner Ville Distribution (WVD) and in [15] the use of the DWT combined with the STFT is employed for the diagnosis of broken bars and stator short-circuits. Although it is stated the potential of the time-frequency techniques for the diagnosis of induction machines under variable loads, the different loads analyzed in [13], [14], [15] can be considered a succession of steady states as the variation of the load conditions is very slow.

In [16] the WVD is employed to diagnose rotor asymmetries in a WRIM under random increasing and decreasing speed ramps which cause a fault frequency change of 1.66 Hz/s. This technique is enhanced for the diagnosis of broken bars in squirrel cage induction machines by adding particle filter to extract the fault component [17] where the machines are subjected to random speed changes with a maximum fault frequency change of 4 Hz/s. However, the WVD is suitable for the analysis of single component frequency signals, as artifacts (not real frequency components) appear when multi frequency signals are analyzed with the WVD. To overcome the problem of the WVD artifacts, in [18] is presented an atom time frequency technique based on the adaptative slope transform to diagnose rotor and stator faults of a WRIM under load oscillations that cause a fault frequency change of 1.66 Hz/s. However, both techniques share the drawback of needing an accurate enough speed reading to perform a reliable diagnosis.

The last time-frequency technique developed for the diagnosis of induction machines operating in variable load conditions is the Harmonic Order Tracking Analysis (HOTA), [19] and [20], which is based on the computation of the Gabor Transform (GT) as in [13]. In [19] an asymmetry in a WRIM under transient conditions, which cause a change in the fault frequency up to 0.26 Hz/s, is diagnosed, whereas in [20] an induction machine fed from a VSD with constant and transient loads is diagnosed for broken bars. However, in [20] the rate of change of the load is not shown. In any case, time frequency analysis techniques based in the STFT, as it is the GT, are not adequate for great frequency changes in the fault frequency.

Finally, other techniques employed for the diagnosis of induction motors under load oscillations are the ones presented in [21], [22], [23], [24], [25], [26], [27]. Some authors propose to analyse the steady state spectrum, but instead of the current, they use different signals as a two-axis rotating current reference frame [26], the active and reactive power [23], the radial leakage flux [25] or leveraging torque and voltage signatures [27]. Problems might arise if these magnitudes are not available for measurement. Time-frequency transforms might also be used in other transient regimes as a direct startup, using the current [24], or other magnitudes as the speed [28]. In [21] the broken bars of induction motors are diagnosed under a slow change in the torque load by computing the instant active and reactive powers of the induction machine. Finally, in [22] a rotor asymmetry in a wound rotor induction generator fed from a VSD is diagnosed by

measuring the DC component of the space vector control when the machine is subjected to a deceleration ramp which causes a change in the fault frequency of 4.44 Hz/s. The major drawback of these two last alternative techniques is that they do not allow the discrimination of the fault.

To develop a global solution, it must be based in the only signal that can always be measured: the stator line current. If a steady state analysis is performed and the speed is not known, even if the harmonic created by the load variation does not overlap with the bar breakage harmonic, both harmonics cannot be distinguished in the current spectrum. In order to properly analyze this phenomena, a time-frequency (t-f) transform is needed (a mathematical transformation that allows to obtain the signal's energy distribution in the t-f plane, showing higher values in the points of the plane where there is a component of the signal with significant amplitude). In particular, the chosen transform must be able to precisely plot both a constant frequency (created by the load oscillation) and a variable frequency (created by the bar breakage), even if they are very close in the t-f plane. In this paper, the use of the Dragon-Transform is proposed. The tool is successfully tested by simulations and experimental tests with machines enduring periodic load fluctuations. The tool allows to avoid false diagnosis due to load oscillations, thanks to precisely tracing both the constant and variable frequencies as very thin lines, enabling a very clear distinction between bar breakages and load oscillations. Even the speed ripple effect caused by the bar breakage can be seen for the first time in the technical literature.

This paper (extended version of [29]), is organized as follows: Section II shows the theory of the Dragon-Transform and its suitability for load oscillations. Section III presents the diagnosis results for simulated signals and Section IV shows the experimental results. Finally, Section V shows the conclusions of this work.

II. DRAGON-TRANSFORM FOR LOAD OSCILLATIONS

As stated in the introduction, time-frequency transforms can be classified in two types: transforms which try to determine the main frequency in a certain frequency band, and transforms which try to plot all the evolutions present in the entire time-frequency plane. In order to obtain the highest amount of information, and better represent the frequency content of the signal and its time evolution, continuous time-frequency transforms are the best option.

Inside this set, transforms are mainly divided in two types: Wigner-Ville distributions (WVD), and atom-based time-frequency transforms. The main problem of the WVD is that cross terms appear when a signal with multiple components is analyzed. Smoothed versions of this transform have been proposed trying to solve this problem. On the other hand, atom-based time-frequency transforms do not produce cross-terms, but the energy of the harmonics appear scattered around their real evolution. In other words, the evolutions, which physically are perfectly thin lines (since for each time instant, a component has only one frequency), they appear represented as lines with a certain thickness.

Dragon-Transform was originally proposed to enable the diagnosis of bar breakages in induction motors started-up with

frequency converters [30]. This is a very difficult problem, since the harmonics describe evolutions which are very close in the t-f plane: a transform able to represent these evolutions as very thin lines is necessary, so they are not mixed up. The Dragon-Transform does not eliminate the energy scattering, it forces the scattering to take place throughout the component evolution. As a result, the evolutions appear as very thin lines, and the problem is solved.

For instance, Fig. 1(a) represents the theoretical evolutions of the harmonics to be captured in an induction motor stator current: the fundamental component traces a horizontal line, while the Lower Sideband Harmonic (LSH) evolves below under a load oscillation (from higher to lower load, since its frequency increases). Below the LSH, a part of the evolution of a secondary asymmetry harmonic can be also observed.

The Dragon-Transform result, shown in Fig. 1(b), shows these evolutions as perfectly thin lines. This is achieved by forcing the dispersion of the energy along the evolution of the current component itself, instead of around it. This is the base proposed in the present paper, to achieve the diagnosis of an induction motor under periodic load oscillations, when the harmonics evolutions can describe very different paths. In the following sections, the capabilities of the transform are tested under load oscillations and bar breakages, using simulation and experimental results.

According to [3], the load torque oscillation can be classified into four types: rotor-position-dependent, single frequency, periodic dip and random dip. The first type introduces speed-dependent harmonics in the stator current spectrum at $(1 \pm k(1-s)/p)f_0$. The second and third type introduce sidebands around the fundamental at $f_0 \pm kf_{osc}$. Finally, in random dip, the frequency of the sidebands is time window dependent.

In the absence of speed-reducing couplings, the sideband frequencies introduced by the first type of oscillating load are sufficiently far away from the rotor asymmetry harmonics, so they pose no problems in differentiating them. However, in the case of the second type of oscillating torque, if the frequency is sufficiently low, the sideband harmonics may appear very close to the rotor asymmetry harmonics, giving rise to false diagnosis. Therefore, in this work, we focus our study only on the single-frequency oscillating load torque: $T_{avg} + T_{osc} \cos(2\pi f_{osc}t)$.

III. SIMULATION RESULTS

The aim of this section is to validate the methodology under a controlled environment, without the impact of lab test factors: non-ideal motor characteristics (as inherent rotor asymmetries), errors from measuring devices (voltage and current errors, or phase differences), and impact of environmental conditions (e.g. changing temperature). Moreover, a model enables to change only one element each simulation, to properly analyze its effect: type of load or number of broken bars. For that, the Dragon-Transform is input with simulated signals from a dynamic model of a 4-pole, 4 kW induction motor (data in Appendix). The model [31], based on the multiple coupled circuit approach, is implemented in MATLAB and solved using a 4th order Runge-Kutta with a step size of 10^{-4} s and the following assumptions: infinite permeability, no saturation, constant air-gap and arbitrary number of spatial harmonics considered in inductance

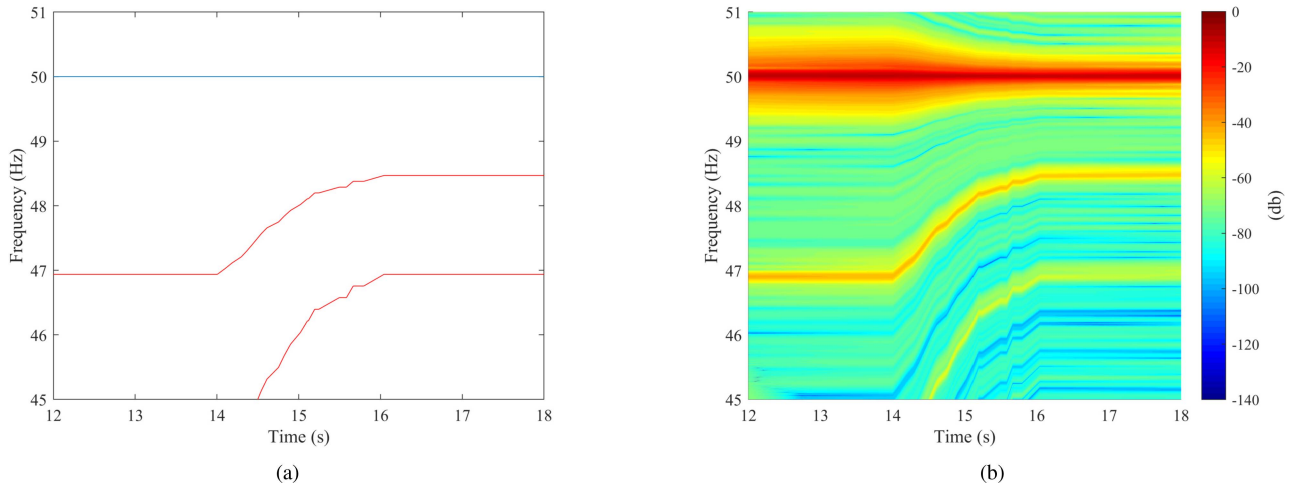


Fig. 1. Theoretical evolutions of the harmonics to be captured (a) and the related Dragon-Transform result (b).

TABLE I
LOAD DESCRIPTION

	Type	Frequency	% of Rated load
L1	Constant	-	100
L2	Sinusoidal	0.3 Hz	75 to 95
L3	Sinusoidal	1.5 Hz	75 to 95

and torque calculations. The broken bar is modeled by increasing its impedance by 10^{12} .

Table I shows the load characteristics of the three cases under analysis (the rest of the model parameters remain unchanged). For each of these three cases, which include constant (L1) and periodic loads (L2, L3), four states are considered: healthy, one broken bar, two broken bars and three broken bars. The resulting simulated currents are then decimated from 10 kHz to 250 Hz (by using decimate Matlab function), and input to the Dragon-Transform along with the simulated slip. Finally, the results are represented in dB with respect to the maximum energy density in the t-f plane, which belongs to the fundamental component.

The Dragon-Transform results are presented in Figs. 2, 3, and 4. In each of these figures, the results for the first three states are represented: healthy (a), one broken bar (b) and two broken bars (c). The fourth state results (three broken bars) are only shown in Section III-C through the quantification indices, since the effects of the increase in fault severity in the t-f plane can already be clearly perceived when going from 1 to 2 broken bars, as discussed in depth below: wider frequency band covered by the LSH (due to a higher speed ripple effect) and higher energy density along its trajectory (due to a higher amplitude of the LSH). The frequency range of analysis has been chosen in such a way that the LSH (Lower Sideband Harmonic) ($f_{LSH} = [1 - 2s]f_0$) is always the lowest harmonic seen in the t-f result. The other two harmonics that are expected to be seen are: the fundamental component at constant f_0 Hz (all cases) and the load oscillation harmonic at constant $f_0 - f_{osc}$ Hz (periodic load cases). Finally, it must be noted that due to the speed oscillations

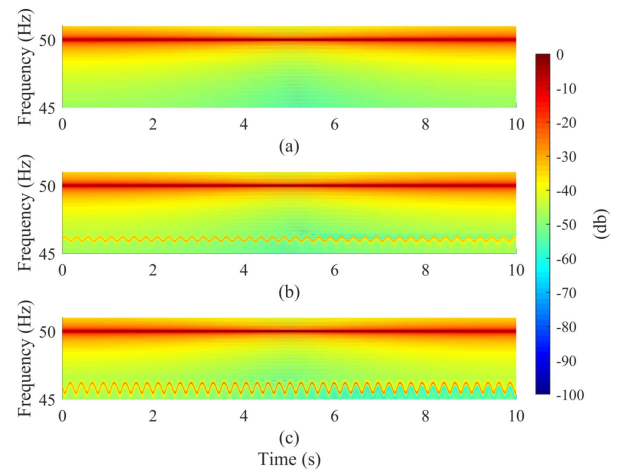


Fig. 2. Simulation results at constant load (L1): healthy (a), one broken bar (b), and two broken bars (c).

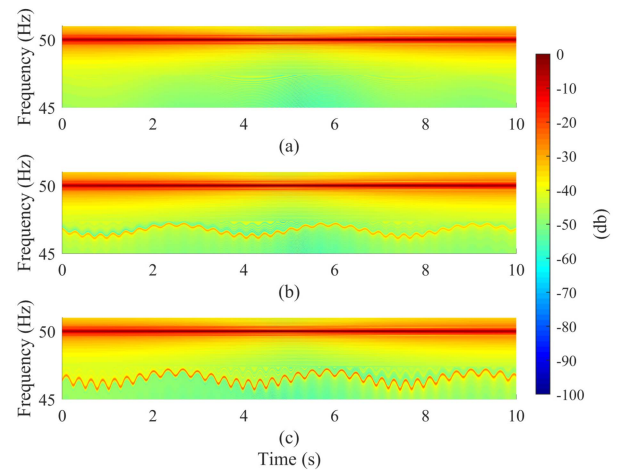


Fig. 3. Simulation results with periodic load (L2): healthy (a), one broken bar (b), and two broken bars (c).

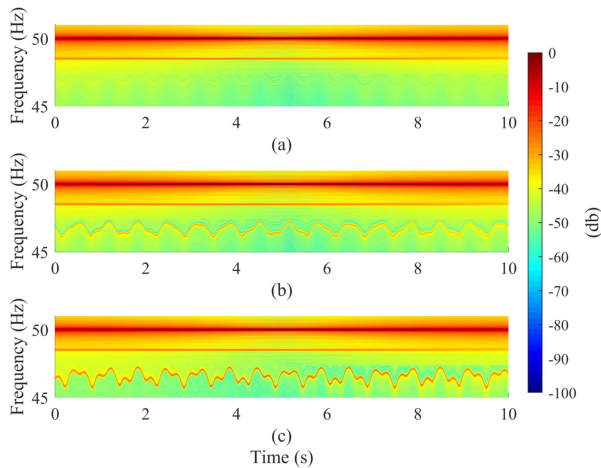


Fig. 4. Simulation results with periodic load (L3): healthy (a), one broken bar (b), and two broken bars (c).

caused by the breakages of the bars, the slip is slightly different between the three states and therefore so is the LSH frequency evolution.

A. Constant Load

Fig. 2 shows the results for the case of constant load. As the fault severity is increased, a pattern is revealed at around 46.7 Hz. This pattern perfectly matches the LSH evolution according to its theoretical formula when the simulated slip is used. Moreover, when comparing Fig. 2(b) (one broken bar) with Fig. 2(c) (two broken bars), it can also be observed how the pattern gets darker (which means more energy), clearly indicating an increase in the severity of the fault. Finally, it must be noted that, although load is constant, the torque ripple caused by the bar breakage creates a periodic oscillation in the motor speed, and therefore, in the LSH frequency. Thanks to the Dragon-Transform, this is the first time in which the LSH evolution is plotted with a precision such that even the speed ripple effect can be observed. Moreover, as the number of broken bar increases, it can be seen that the LSH frequency covers a wider band, due to a higher speed oscillation.

B. Periodic Load

Figs. 3 and 4 show the results for the cases of periodic load oscillations. In all of them, the appearance of the pattern can be perceived, as well as the difference between the three states. In Fig. 3(b), the LSH frequency periodically changes in time, following two patterns: one slow caused by the load oscillation, and a second fast superimposed, created by the speed ripple effect, whose amplitude increases when the second bar is broken (Fig. 3(c)). Periodicity is also present in Fig. 4, but is harder to see, since both the load oscillation and the speed ripple effect change at a high rate, and when superimposed, create a seemingly more chaotic pattern. Furthermore, in Fig. 4, the load oscillation harmonic can also be clearly perceived at a constant 48.5 Hz. In the other case, this harmonic appears at 49.7 Hz.

C. Amplitude Quantification

Table II shows the mean value of the LSH amplitude (in dB with respect to the fundamental component) for each case and

TABLE II
MEAN VALUE OF LSH AMPLITUDE (IN DB WITH RESPECT TO THE FUNDAMENTAL COMPONENT) FOR EACH CASE ANALYZED

	L1	L2	L3
Healthy	-45.82	-44.35	-45.06
1 broken bar	-30.09	-31.38	-31.42
2 broken bars	-24.99	-24.31	-24.34
3 broken bars	-20.93	-21.71	-21.69



Fig. 5. Experimental setup for the standard squirrel cage induction motor: function generator (1), control unit of the magnetic powder brake (2), DAQ (3), magnetic powder brake (4), tested motor (5), and DC supply source (6).

state analyzed. This value is obtained by computing the average of the maximum energy densities found in a frequency band (0.2 Hz) centered at the exact position of the LSH at each time instant. For all cases, as fault severity increases, amplitude increases, showing its great usefulness as a diagnostic tool.

IV. EXPERIMENTAL RESULTS

Two different test benches have been used to validate the approach through experimental results: a standard squirrel cage induction machine in motor mode (Section IV-A) and a BKB universal machine working as a wounded rotor induction generator (Section IV-B).

A. Squirrel Cage Induction Motor

In order to evaluate the methodology when the machine is operating in motor mode, the experimental setup shown in Fig. 5 has been used. It consists of a controllable magnetic powder brake coupled to a 0.75 kW induction machine (see appendix for its characteristics). To create the periodic oscillating load torque, a waveform generator is used to input a sinusoidal voltage of a certain amplitude and frequency to the magnetic powder brake control unit. The characteristics of the loads are equivalent to those of L1, L2 and L3 from Table I (simulation results). For each of these loads, three states are considered: healthy, one broken bar and three broken bars.

As for the acquisition system, speed is measured using a 500-line incremental encoder installed on the non-drive end of the induction machine and powered by a dc supply source, while the current is measured using a current probe (YHDC-SCT013). Both signals are simultaneously recorded using an oscilloscope (PicoTech 4262) at 200 kHz during 10 s. The acquired signals are then decimated to 250 Hz and input to the Dragon-Transform. Finally, as in Section III, the results are represented in dB with respect to the maximum energy density in the t-f plane, which belongs to the fundamental component.

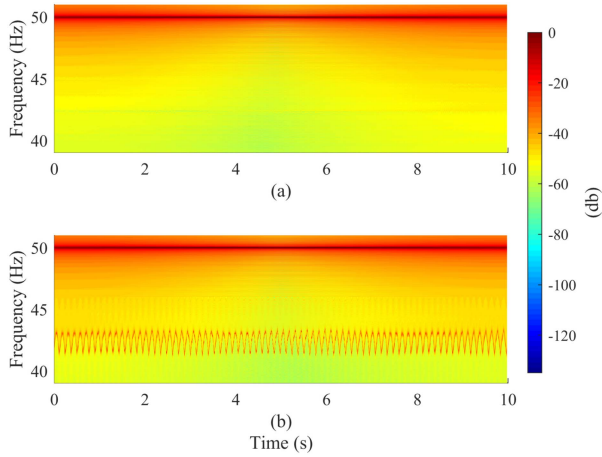


Fig. 6. Experimental results at constant load (L1): healthy (a) and three broken bars (b).

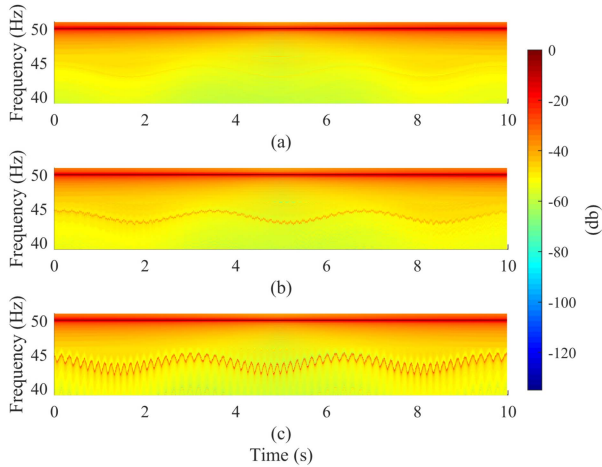


Fig. 7. Experimental results with periodic load (L2): healthy (a), one broken bar (b), and three broken bars (c).

TABLE III

MEAN VALUE OF LSH AMPLITUDE (IN DB WITH RESPECT TO THE FUNDAMENTAL COMPONENT) FOR EACH EXPERIMENTAL CASE ANALYZED

	L1	L2	L3
Healthy	-50.93	-47.50	-46.26
One broken bar	x	-37.83	-37.34
Three broken bars	-25.28	-26.37	-26.58

The Dragon-Transform results are presented in Figs. 6, 7, and 8 and Table III. Differences in the LSH quantification are to be expected between simulation and experimental results, since, although of similar size, the motors are different, with different parameters (inertia, stator resistance, etc.): approximately 6 dB difference with 1 broken bar and 5 dB with 3 broken bars (same for all transients). Despite this, the shape of the t-f evolutions are very similar, and the same conclusions can be extracted. Summarizing:

- The speed ripple effect can be seen even under constant load when the bar breakage takes place (Fig. 6(b)), which enables to distinguish the fault from a perfectly periodic load oscillation frequency.

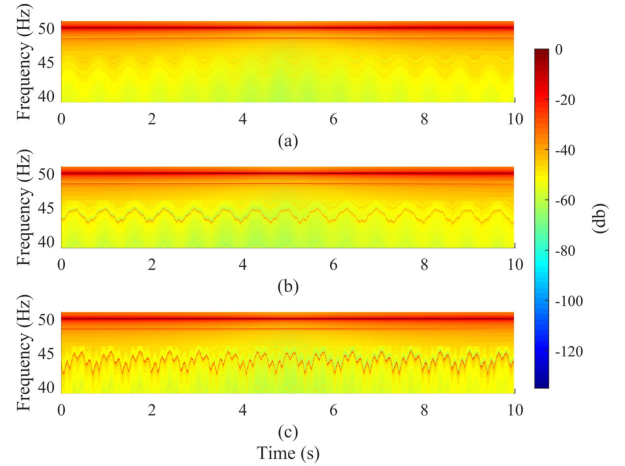


Fig. 8. Experimental results with periodic load (L3): healthy (a), one broken bar (b), and three broken bars (c).

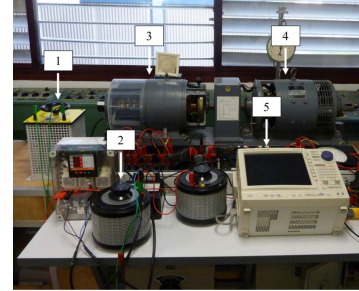


Fig. 9. Experimental setup for the wounded rotor induction generator: fault resistance (1), motorised rheostat (2), tested machine (3), DC machine (4), and DAQ (5).

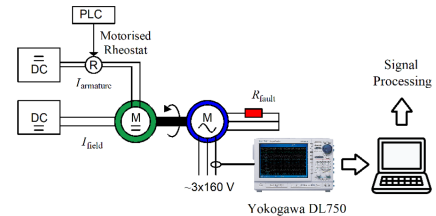


Fig. 10. Diagram of the experimental setup for the wounded rotor induction generator.

- The energy of the faulty harmonic increases with the fault severity: it gets darker. As in simulation, this is also confirmed when the quantification of the mean value of the LSH amplitude is performed (see Table III).
- The speed ripple effect is superimposed to the speed oscillation caused by the single frequency load torque oscillation. This is particularly clear in Fig. 7(c).
- The speed-independent harmonic caused by the periodic load oscillation is shown as a horizontal line, clearly seen below the fundamental component in Fig. 8.

B. Wounded Rotor Induction Generator

To validate the methodology when a machine is operating in generator mode, a BKB universal machine acting as a wounded rotor induction generator is tested (see appendix for its characteristics and Figs. 9 and 10 for a picture and a diagram of the test experimental setup). A DC machine moves the rotor

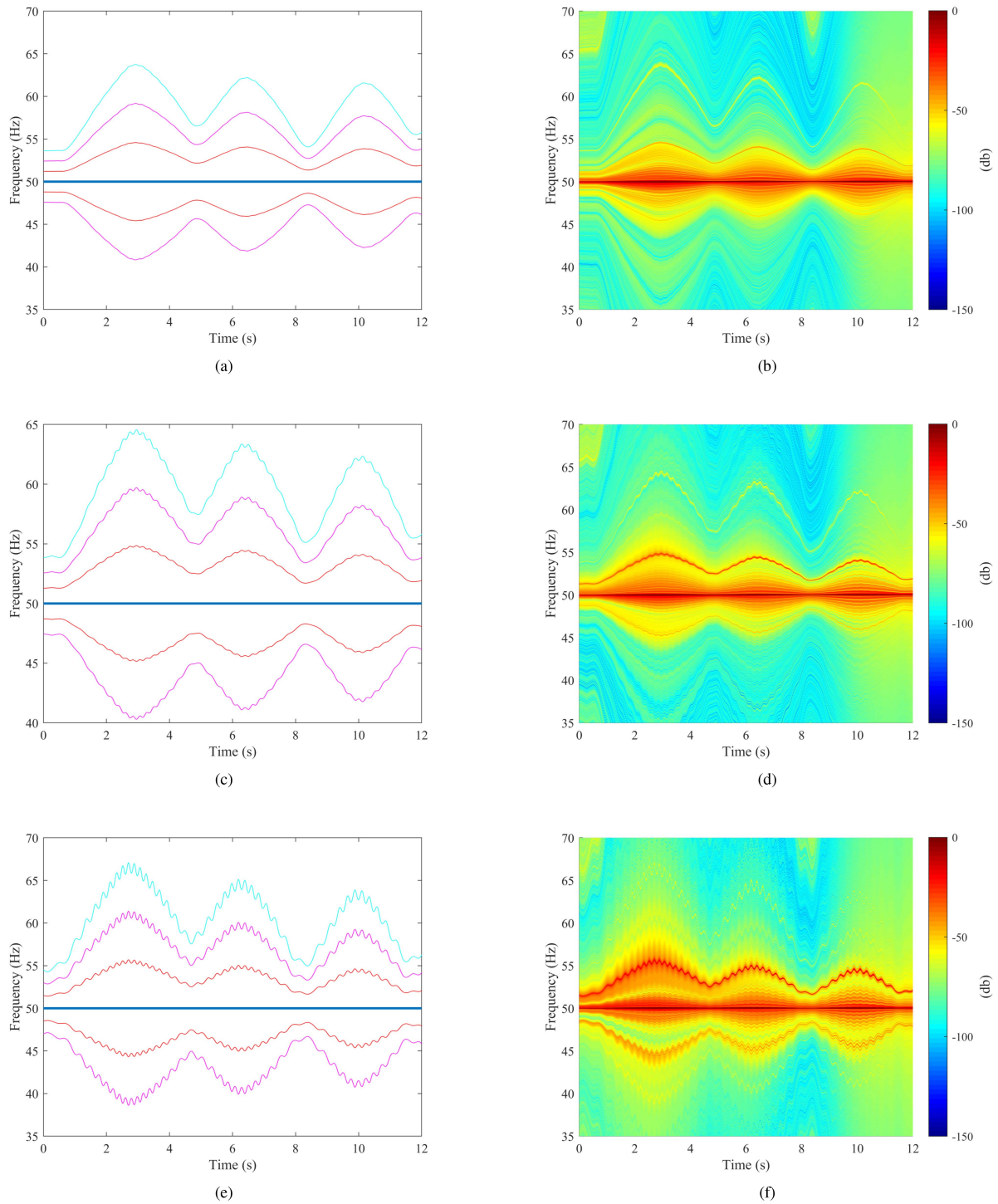


Fig. 11. Theoretical evolutions and Dragon-Transform results for the BKB universal machine working as induction generator: healthy (a)–(b), $\Delta R = 15.73\%$ (c)–(d), and $\Delta R = 94.33\%$ (e)–(f).

over the synchronous speed to achieve generator mode. The DC machine is controlled to perform during each test the same speed fluctuations. Yet, when the asymmetry appears, speed ripple takes place. Rotor and stator are primary and secondary windings respectively. The primary winding is connected to a three-phase supply source of 160 V, and its current is measured to perform diagnosis. The secondary winding is short-circuited, while additional resistances are connected in series to a phase, simulating up to 9 different degrees of asymmetry. The fault

severity is given by the percentage of the fault resistance over the phase resistance ($\Delta R = R_{fault}/R_{phase} \cdot 100$). This test is equivalent to a wounded rotor induction generator with a rotor fault.

The theoretical evolutions of the harmonics for the cases of $\Delta R = 0\%$ (healthy), $\Delta R = 15.73\%$ (fifth fault state) and $\Delta R = 94.33\%$ (last fault state) are shown in Fig. 11(a), (c), and (e): fundamental component evolution is plotted, together with the rotor asymmetry harmonics with frequencies

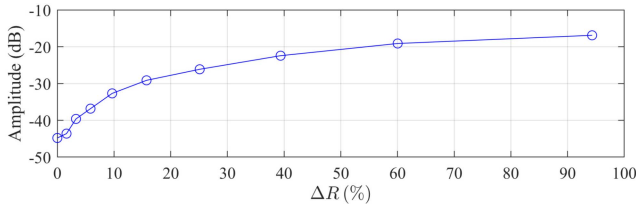


Fig. 12. Mean value of LSH amplitude (in dB with respect to the fundamental component) for each case analyzed.

$f = (1 \pm 2ks)f_0$, being s the slip, f_0 the main supply frequency and k a positive integer, which in this case is equal to 1, 2 and 3 (the last number, only for the negative sign). Faulty case plotted in Fig. 11(c) shows the appearance of a speed ripple effect (the oscillation superimposed on the one created by the load oscillation), caused by the asymmetry in the secondary winding. As shown in Fig. 11(e), this ripple increases with the fault severity.

Fig. 11(b), (d) and (f) show the Dragon-Transform results for these three cases, while Fig. 12 shows the quantification of the LSH amplitude for all cases, obtained as in Sections III and IV-A, when analyzing the primary winding currents. In the three cases, the fundamental component appears as a very clear horizontal line. Due to the precision of the transform used, the LSH appears even in the healthy case (Fig. 11(b)). Its trajectory is at higher frequencies than the fundamental component, since the machine is operating as a generator. In the faulty cases, its amplitude highly increases (from -45 to -17 dB, see Fig. 12). Moreover, up to five faulty harmonics are detected in the most severe case (Fig. 11(f)). Finally, this, along with the results presented in the previous subsection, are the first results in which the trajectories are plotted in such a precision that even the oscillations caused by ripple effect can be observed. All this enhances the reliability of the diagnosis performed.

V. CONCLUSION

The use of the Dragon-Transform has been proposed for the diagnosis of induction motors under periodic load oscillations. Thanks to the transform capabilities, the evolutions of the faulty harmonics can be observed in the t-f plot as very thin lines, together with the constant frequency introduced by the load oscillation. The transform performs very different analysis adapted to the type of evolution of the harmonic to be captured, simultaneously plotting the different components of the current in a single figure. Even if the bar breakage harmonics have changing frequencies, while the periodic load oscillations create constant frequencies, the transform results enable to perfectly plot them, and distinguish between both phenomena. Both simulation and laboratory test generate the same results when performed in the same conditions, highly validating the precision of the evolutions obtained, which perfectly match theory predictions. For the first time in the technical literature, it can be seen how, when the fault appears, speed ripple effect takes place, and high frequency oscillations are superimposed with the original trajectory of the harmonics. Up to five faulty harmonics evolutions are depicted with high precision, which enables a very reliable diagnosis.

APPENDIX A

Simulated motor characteristics:

- $P_N = 4$ kW, $U_N = 400$ V, star connection, $p = 2$, $T_N = 26.6$ N · m.
- $N_{bars} = 28$, $J = 0.03$ kg · m².
- $R_{st} = 1.25$ Ω, $L_{\sigma,st} = 3.57$ mH, $L_{\mu,st} = 191.4$ mH.
- $R_{bar} = 70$ μΩ, $L_{\sigma,bar} = 0.28$ μH, $L_{\mu,bar} = 5.6$ μH, $R_{end-ring\ segment} = 1.8$ μΩ, $L_{\sigma,end-ring\ segment} = 1.8$ nH.

BKB machine characteristics:

- $P_N = 1.5$ kW, $f_N = 50$ Hz, $p = 1$, $n_N = 3200$ rpm (working as a generator).
- *Stator Winding*: $U_N = 240$ V, $I_N = 5.5$ A, star connection, $R_{st} = 4.4$ Ω per phase.
- *Rotor Winding*: $I_N = 8$ A, delta connection, $R_{rot} = 10.15$ Ω per phase.

Standard squirrel cage motor characteristics:

- $P_N = 0.75$ kW, star connection.
- $U_N = 400$ V, $I_N = 1.86$ A, $n_N = 1395$ rpm, $T_N = 5.13$ N · m.

REFERENCES

- [1] *Encyclopedia of Electrical and Electronic Power Engineering*. Amsterdam, The Netherlands: Elsevier, 2023.
- [2] J. Bonet-Jara, A. Quijano-Lopez, D. Morinigo-Sotelo, and J. Pons-Llinares, "Sensorless speed estimation for the diagnosis of induction motors via MCSA. review and commercial devices analysis," *Sensors*, vol. 21, no. 15, 2021, Art. no. 5037. [Online]. Available: <https://www.mdpi.com/1424-8220/21/15/5037>
- [3] L. Wu, T. G. Habetler, and R. G. Harley, "A review of separating mechanical load effects from rotor faults detection in induction motors," in *Proc. IEEE Int. Symp. Diagn. Electric Mach. Power Electron. Drives*, 2007, pp. 221–225.
- [4] A. Stefani, A. Bellini, and F. Filippetti, "Diagnosis of induction machines' rotor faults in time-varying conditions," *IEEE Trans. Ind. Electron.*, vol. 56, no. 11, pp. 4548–4556, Nov. 2009.
- [5] Y. Gritli, A. Stefani, C. Rossi, F. Filippetti, and A. Chatti, "Experimental validation of doubly fed induction machine electrical faults diagnosis under time-varying conditions," *Electric Power Syst. Res.*, vol. 81, no. 3, pp. 751–766, 2011.
- [6] Y. Gritli, C. Rossi, L. Zarri, F. Filippetti, A. Chatti, and D. Casadei, "Double frequency sliding and wavelet analysis for rotor fault diagnosis in induction motors under time-varying operating condition," in *Proc. IEEE 8th Symp. Diagn. Elect. Mach. Power Electron. Drives*, 2011, pp. 676–683.
- [7] Y. Gritli, L. Zarri, C. Rossi, F. Filippetti, G.-A. Capolino, and D. Casadei, "Advanced diagnosis of electrical faults in wound-rotor induction machines," *IEEE Trans. Ind. Electron.*, vol. 60, no. 9, pp. 4012–4024, Sep. 2013.
- [8] Y. Gritli et al., "Advanced diagnosis of broken bar fault in induction machines by using discrete wavelet transform under time-varying condition," in *Proc. IEEE Int. Electric Mach. Drives Conf.*, 2011, pp. 424–429.
- [9] Y. Gritli, S. B. Lee, F. Filippetti, and L. Zarri, "Advanced diagnosis of outer cage damage in double-squirrel-cage induction motors under time-varying conditions based on wavelet analysis," *IEEE Trans. Ind. Appl.*, vol. 50, no. 3, pp. 1791–1800, May/Jun. 2014.
- [10] S. H. Kia, H. Henao, and G.-A. Capolino, "Windings monitoring of wound rotor induction machines under fluctuating load conditions," in *Proc. IEEE 37th Annu. Conf. Ind. Electron. Soc.*, 2011, pp. 3459–3465.
- [11] F. Vedreño-Santos, M. Riera-Guasp, H. Henao, M. Pineda-Sánchez, and J. A. Antonino-Daviu, "Diagnosis of eccentricity in induction machines working under fluctuating load conditions, through the instantaneous frequency," in *Proc. IEEE 38th Annu. Conf. Ind. Electron. Soc.*, 2012, pp. 5108–5113.
- [12] F. Vedreño-Santos, M. Riera-Guasp, H. Henao, M. Pineda-Sánchez, and R. Puche-Panadero, "Diagnosis of rotor and stator asymmetries in wound-rotor induction machines under nonstationary operation through the instantaneous frequency," *IEEE Trans. Ind. Electron.*, vol. 61, no. 9, pp. 4947–4959, Sep. 2014.

- [13] B. Yazici and G. Kliman, "An adaptive statistical time-frequency method for detection of broken bars and bearing faults in motors using stator current," *IEEE Trans. Ind. Appl.*, vol. 35, no. 2, pp. 442–452, Mar./Apr. 1999.
- [14] M. Blodt, D. Bonacci, J. Regnier, M. Chabert, and J. Faucher, "On-line monitoring of mechanical faults in variable-speed induction motor drives using the Wigner distribution," *IEEE Trans. Ind. Electron.*, vol. 55, no. 2, pp. 522–533, Feb. 2008.
- [15] J. Cusidó, L. Romeral, J. A. Ortega, J. A. Rosero, and A. G. Espinosa, "Fault detection in induction machines using power spectral density in wavelet decomposition," *IEEE Trans. Ind. Electron.*, vol. 55, no. 2, pp. 633–643, Feb. 2008.
- [16] V. Climente-Alarcon, M. Riera-Guasp, J. Antonino-Daviu, J. Roger-Folch, and F. Vedreñ-Santos, "Diagnosis of rotor asymmetries in wound rotor induction generators operating under varying load conditions via the Wigner-Ville distribution," in *Proc. Int. Symp. Power Electron. Power Electron. Elect. Drives Automat. Motion*, 2012, pp. 1378–1383.
- [17] V. Climente-Alarcon, J. A. Antonino-Daviu, A. Haavisto, and A. Arkkio, "Particle filter-based estimation of instantaneous frequency for the diagnosis of electrical asymmetries in induction machines," *IEEE Trans. Instrum. Meas.*, vol. 63, no. 10, pp. 2454–2463, Oct. 2014.
- [18] J. Pons-Llinares, M. Riera-Guasp, J. A. Antonino-Daviu, and F. Vedreñ-Santos, "Transient diagnosis of induction generators via atom-based time-frequency transforms," in *Proc. Int. Conf. Elect. Mach.*, 2014, pp. 1793–1799.
- [19] A. Sapena-Bano, M. Riera-Guasp, R. Puche-Panadero, J. Martinez-Roman, J. Perez-Cruz, and M. Pineda-Sanchez, "Harmonic order tracking analysis: A speed-sensorless method for condition monitoring of wound rotor induction generators," *IEEE Trans. Ind. Appl.*, vol. 52, no. 6, pp. 4719–4729, Nov./Dec. 2016.
- [20] A. Sapena-Bano, J. Burriel-Valencia, M. Pineda-Sanchez, R. Puche-Panadero, and M. Riera-Guasp, "The harmonic order tracking analysis method for the fault diagnosis in induction motors under time-varying conditions," *IEEE Trans. Energy Convers.*, vol. 32, no. 1, pp. 244–256, Mar. 2017.
- [21] S. M. A. Cruz, "An active-reactive power method for the diagnosis of rotor faults in three-phase induction motors operating under time-varying load conditions," *IEEE Trans. Energy Convers.*, vol. 27, no. 1, pp. 71–84, Mar. 2012.
- [22] Y. Gritli, C. Rossi, D. Casadei, F. Filippetti, and G.-A. Capolino, "A diagnostic space vector-based index for rotor electrical fault detection in wound-rotor induction machines under speed transient," *IEEE Trans. Ind. Electron.*, vol. 64, no. 5, pp. 3892–3902, May 2017.
- [23] M. Drif, H. Kim, J. Kim, S. B. Lee, and A. J. M. Cardoso, "Active and reactive power spectra-based detection and separation of rotor faults and low-frequency load torque oscillations," *IEEE Trans. Ind. Appl.*, vol. 53, no. 3, pp. 2702–2710, May/June 2017.
- [24] H. Kim, S. B. Lee, S. Park, S. H. Kia, and G.-A. Capolino, "Reliable detection of rotor faults under the influence of low-frequency load torque oscillations for applications with speed reduction couplings," *IEEE Trans. Ind. Appl.*, vol. 52, no. 2, pp. 1460–1468, Mar./Apr. 2016.
- [25] T. Goktas, M. Arkan, M. S. Mamis, and B. Akin, "Separation of induction motor rotor faults and low frequency load oscillations through the radial leakage flux," in *Proc. IEEE Energy Convers. Congr. Expo.*, 2017, pp. 3165–3170.
- [26] M. Hoseintabar Marzebali, R. Bazghandi, and V. Abolghasemi, "Rotor asymmetries faults detection in induction machines under the impacts of low-frequency load torque oscillation," *IEEE Trans. Instrum. Meas.*, vol. 71, 2022, Art. no. 3522011.
- [27] T. Goktas, M. Arkan, M. Zafarani, and B. Akin, "Separation harmonics for detecting broken bar fault in case of load torque oscillation," in *Proc. IEEE Int. Electric Mach. Drives Conf.*, 2015, pp. 1452–1458.
- [28] T. A. Garcia-Calva, D. Morinigo-Sotelo, V. Fernandez-Cavero, A. Garcia-Perez, and R. D. J. Romero-Troncoso, "Early detection of broken rotor bars in inverter-fed induction motors using speed analysis of startup transients," *Energies*, vol. 14, no. 5, 2021, Art. no. 1469. [Online]. Available: <https://www.mdpi.com/1996-1073/14/5/1469>
- [29] J. Bonet-Jara, V. Fernandez-Cavero, F. Vedreño-Santos, and J. Pons-Llinares, "Very accurate time-frequency representation of induction motors harmonics for fault diagnosis under arbitrary load variations," in *Proc. Int. Conf. Elect. Mach.*, 2022, pp. 1517–1523.
- [30] V. Fernandez-Cavero, J. Pons-Llinares, O. Duque-Perez, and D. Morinigo-Sotelo, "Detection of broken rotor bars in nonlinear startups of inverter-fed induction motors," *IEEE Trans. Ind. Appl.*, vol. 57, no. 3, pp. 2559–2568, May/June 2021.

- [31] J. Bonet-Jara, D. Morinigo-Sotelo, O. Duque-Perez, L. Serrano-Iribarnegaray, and J. Pons-Llinares, "End-ring wear in deep-well submersible motor pumps," *IEEE Trans. Ind. Appl.*, vol. 58, no. 4, pp. 4522–4531, Jul./Aug. 2022.



Jorge Bonet-Jara received the Engineer's degree in industrial engineering, the master's degree in industrial engineering with specialization in electrical engineering, and the Ph.D. degree in electrical engineering from the Universitat Politècnica de València, València, Spain, in 2016, 2018, and 2023, respectively. He is currently a Postdoctoral Researcher. His research interests include SPTH, machine modeling, fault diagnosis, condition monitoring, and sensorless speed estimation.



Vanessa Fernandez-Cavero received the B.S. degree in industrial organization engineering and electrical engineering from the ICAI, Comillas Pontifical University, Madrid, Spain, in 2005, and the Ph.D. degree in electrical engineering from the University of Valladolid, Valladolid, Spain, in 2018. She is currently a Professor with the University of Burgos, Burgos, Spain. Her research interests include monitoring of induction machines, detection, and diagnosis of faults in inverter-fed IM in transient regimes.



Francisco Vedreño-Santos received the M.Sc. degree in electrical engineering, the second M.Sc. degree in energy technologies for sustainable development, and the Ph.D. degree in electrical engineering from the Universitat Politècnica de València (UPV), València, Spain, in 2008, 2012, and 2013, respectively. He is currently a Lecturer of electronic & electrical engineering with the School of Computing, Engineering & Built Environment, Edinburgh Napier University, Edinburgh, U.K. His research interests include diagnostics, signal processing and condition

monitoring of electric machines, and design and control of power electronics for wind power applications.



Daniel Morinigo-Sotelo (Member, IEEE) received the B.S. and Ph.D. degrees in electrical engineering from the University of Valladolid, Valladolid, Spain, in 1999 and 2006, respectively. From 2000 to 2015, he was a Research Collaborator on Electromagnetic Processing of Materials with the Light Alloys Division of CIDAUT Foundation. He is currently with the Research Group ADIRE, which belongs to the ITAP Institute (UVA), and with the HSPdigital Research Group, México. His research interests include fault detection and diagnostics of induction machines,

power quality, and smart grids.



Joan Pons-Llinares (Member, IEEE) received the M.Sc. degree in industrial engineering and the Ph.D. degree in electrical engineering from the Universitat Politècnica de València (UPV), València, Spain, in 2007 and 2013, respectively. He is currently an Associate Professor with the Electric Engineering Department, UPV. His research interests include time-frequency transforms, condition monitoring, and efficiency estimation of electrical machines.